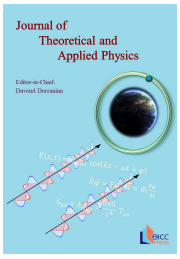

Volume 17, Issue 2, 172317 (1-8)

Journal of Theoretical and Applied Physics (JTAP)

https://dx.doi.org/10.57647/j.jtap.2023.1702.17

Theoretical study of conduction intra-subband nonlinear optical absorption and donor-impurity ionizing energy associated with lowest excited-states in single InGaN-based quantum well with a novel modified potential

Redouane En-nadir[1]*, Haddou El-ghazi[1,2]

[1]*LPS, Faculty of sciences, University of Sidi Mohamed Ben Abdullah, Fez, Morocco.*
[2]*ENSAM, University Hassan-II, Casablanca, Morocco.*

***Corresponding author**: redouane.en-nadir@usmba.ac.ma

Received 21 September 2022; Accepted 06 January 2023; Published online 10 January 2023

Abstract:
This paper provides a theoretical investigation of the ground and first excited-states donor impurity binding energy and the linear and nonlinear optical absorption coefficients in quantum well with novel modulated potential called Redouane-Haddou potential (RHP). Within the effective-mass theory, the Schrödinger equation has been calculated numerically using the finite element method. The analytical expressions of the optical absorption coefficients are obtained within compact density matrix theory. Our results reveal that the *A*-parameter has a significant influence on the confinement profile and electron states, therefore, the binding energy as well as the optical properties of the investigated system. It increases the binding energy and redshift (blueshift) associated with drop (improve) of the linear and nonlinear optical absorption coefficients related to 2p→1s, 2p→2s, and 3s→2p transitions. Moreover, it is noticed that with an appropriate choice of the *A*-parameter and structure dimension, the optical response of the investigated system can be tailored in a controllable manner.

Keywords: Binding energy; Optical absorption; RHP potential; Quantum well

1. Introduction

Rapid development in sophisticated nanotechnology has enabled the growth of low-dimensional systems with fascinating electronic and optical properties. These structures attracted special and increasing attention due to their extensive applications areas such as electronic, optoelectronic devices technology [1–6]. Nowadays, advances in materials growth techniques make it possible to grow quantum wells (QWs) with varying confinement potentials, symmetrical or asymmetrical with respect to the center of the well. Various potentials such as Gaussian, Tietz-Hua, Razavy, Morse, Mathieu, etc. have been widely used in material science physics to specify realistic confinement of charge carriers [7–11]. In this context, the potential modulated by my supervisor and myself (i.e., Redouane-Haddou potential or RHP) is a novel interesting function to represent the confinement effect in QWs with an adaptable geometry. Besides, it is well known that the presence of defects and impurity states affects considerably the electrical and optical features of nanomaterials, and it is more pronounced than their 'bulk' counterparts [12]. Hence, it is important to figure out deeply the impurities-related influences on the semiconductor nanostructures in order to govern the performance of electronic and optoelectronic devices. Along with the knowledge that binding energy and optical properties change in multilayered heterostructures, a suitable theory for electronic and optical characteristics of nanostructures can be established with a practical model taking into account different potential profiles. Thus, intensive research

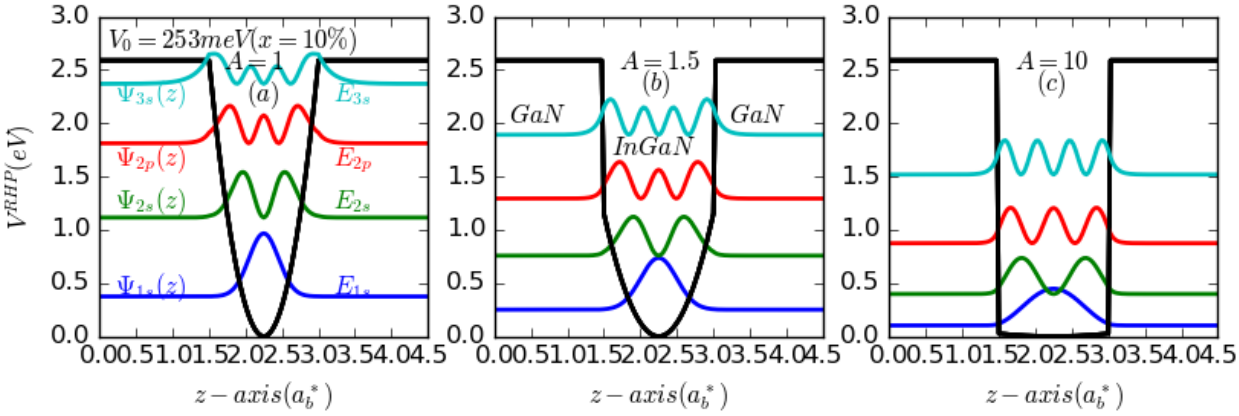

Figure 1. Potential profile and the electron wave functions of the lowest and low-lying states in InGaN/GaN QW versus z-axis for three different values of A-parameter for l=L=1.5.

has been carried out for a better understanding of the physical properties of impurities in QWs [13–18].

Recently, Al et al. have investigated the influence of position dependent effective mass on impurity binding energy and absorption in quantum wells with the Konwent potential [19]. Ungan et al. have reported a study of effects of an intense, high-frequency laser field on the ISB transitions and donor impurity binding energy in quantum wells [20]. The effects of hydrostatic pressure and temperature on the binding energy and optical absorption of a multilayer quantum dot with parabolic confinement have been studied by Ortakaya and coworkers [21]. Bekir et al. have demonstrated the binding energy and wave functions of the 1s, 1p, 1d and 1f energy states of a spherical quantum dot (QD) with parabolic potential [22]. Moreover, Kirak et al. have investigated the impact of an external applied electric field on the electronic properties of the ground and excited states and on the linear and nonlinear optical properties (i.e., absorption coefficients and refractive indices) in a spherical quantum dot considering parabolic confinement with an on-center shallow hydrogenic impurity [23]. In our work recently published in 2021, we investigated theoretically the total absorption coefficient related to inter conduction ISB optical transitions in symmetric In.1Ga.9N/GaN double rectangular quantum wells [24]. However, this study is devoted to investigate shallow donor impurity binding energy of the ground (1s-state) and first excited-state (2-state) and intra-conduction subband (ISB) linear and third-nonlinear and total optical absorption coefficients (i.e., LOAC, NLOAC and TOAC), respectively related to 2p→1s, 2p→2s, and 3s→2p transitions considering the effect of the A-parameter. This later called confinement potential adaptation parameter; it transforms confinement profile from a parabolic shape to the rectangular one with increasing the value of the A-parameter. Our calculations have been performed within the effective-mass approximation using the Finite Element Method (FEM) for many reasons: FEM allows easier modeling of complex geometric and irregular shapes and allows us to critically investigate factors that can affect all complex structures. It allows us to use boundary conditions to define the conditions the model must meet, including point forces, distributed forces, electrical and thermal effects (such as temperature changes, applied external and internal forces, ...) and position constraints. Compared to conventional methods such as variational approach and perturbation method, FEM is more precise and accurate, especially when considering a finite potential barrier which offers the possibility to tunnel through the barriers to the particles (electron, hole) where the analytical solutions become almost impossible with a high degree of freedom (in the case of a non-separable system). Unlike, the effective-mass approximation has been used extensively to describe particle (electron, hole) motion near band extremes (wave vector, K∼0) in the presence of slowly varying weak perturbation, such as applied electric and magnetic fields, especially for shallow-impurities issues in semiconductors. Compared to variational and other conventional methods, it is a very accurate method for the boundary conditions problems, ie. how to connect the solutions on either side of an atomically abrupt interface. In addition, the advent of quantum wells nanostructures brought about a hiatus in the development of effective-mass theory from the well-understood regime of

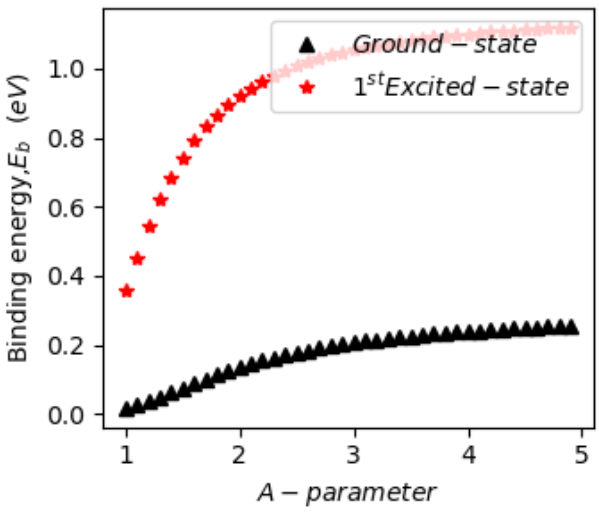

Figure 2. Binding energy of the ground and first excited states of an on-center donor impurity in InGaN/GaN QW as a function of the A-parameter for l=L=1.5.

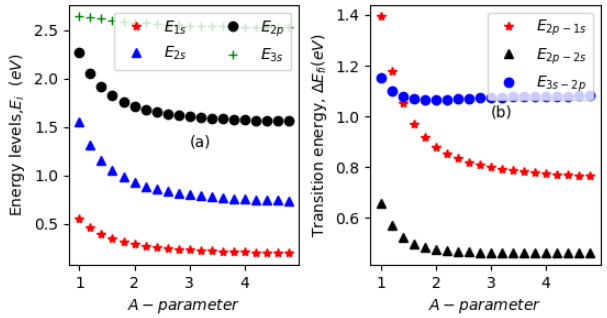

Figure 3. Energy levels and transition energy of electron within the conduction band of InGaN/GaN QW as a function of the A-parameter. Without impurity and for l=L=1.5.

weak perturbation in bulk crystals to the little-understood robust perturbation regime in microstructures [25].

2. Theory and methods

In this study, we consider a Hydrogen-like donor impurity located at the center of a rectangular QW made out of unstrained (m-plan) GaN/InGaN/GaN nanostructure. Within the framework of the effective-mass approximation and without electron–phonon interaction, the electron Hamiltonian in the presence of an impurity is expressed as follows,

$$\mathbf{H} = -\frac{\hbar^2}{2m^*}\boldsymbol{\nabla} + V^{\mathrm{RHP}}(A,z) - \frac{e^2}{\varepsilon_r^*|\mathbf{r}-\mathbf{r}_0|} \tag{1}$$

In this case, the energy levels E_i and their associated wave functions ψ_i are numerically calculated using the one-dimensional Schrodinger equation that can be written as follows,

$$-\frac{\hbar^2}{2m^*}\frac{d^2\psi_i(z)}{dz^2} + \left(V^{\mathrm{RHP}}(A,z) - \frac{e^2}{\varepsilon_r^*|\mathbf{r}-\mathbf{r}_0|}\psi_i(z)\right) = E_i\psi_i(z) \tag{2}$$

where $\hbar$, and e are respectively the Planck constant, electron charge. ε_r^* and m^* are the relative dielectric constant and the conduction band electron-mass of InGaN and GaN. The dependence of these last parameters on the concentration of indium is given as follows [26]:

$$\varepsilon^*_{\mathrm{InGaN}} = \begin{cases} \varepsilon^*_{\mathrm{GaN}} + 6.4x & \text{In the well region} \\ \varepsilon^*_{\mathrm{GaN}} & \text{Elsewhere} \end{cases} \tag{3}$$

$$m^*_{\mathrm{InGaN}} = \begin{cases} 0.1m^*_{\mathrm{InN}} + 0.9m^*_{\mathrm{GaN}} & \text{In the well region} \\ m^*_{\mathrm{GaN}} & \text{Elsewhere} \end{cases} \tag{4}$$

The electron effective-mass is given as m^*_{GaN}=0.20 m_0 and m^*_{InN}=0.11 m_0 (where m_0 denotes the electron mass in vacuum) and the mean relative dielectric constants of GaN and InN respectively are 9.8 ε_0 and 10.5 ε_0 (where ε_0 is the permittivity of free space) [27], [28]. At the interfaces between the well (InGaN) and the barrier (GaN), we assumed that the dielectric constant is equal to the square root of the dielectric constants of both InGaN and GaN ($\sqrt{\varepsilon^*_{\mathrm{InGaN}} \times \varepsilon^*_{\mathrm{GaN}}}$).

The A-parameter dependent finite confinement potential ($V^{\mathrm{RHP}}(A,z)$) is modulated as follows:

$$V^{\mathrm{RHP}}(A,z) = \begin{cases} V_0 & \text{In the barrier regions} \\ \frac{4V_0}{(A\cdot l)^2} \times [z - L - \frac{l}{2}]^2 & \text{In the well region} \end{cases} \tag{5}$$

where L and l are the barriers/well thicknesses, respectively. V_0=0.7 ΔE_g with $\Delta E_g = E_g^{\mathrm{GaN}} - E_g^{\mathrm{InGaN}}$.

$$E_g^{\mathrm{InGaN}} = 0.1E_g^{\mathrm{InN}} + 0.9E_g^{\mathrm{GaN}} + 3.42 \tag{6}$$

Energy band gaps of both GaN and InN materials are equal to 3.51 and 0.70 eV, respectively [29].
The ground-state shallow-donor the binding energy is defined as the difference in energy in the case without impurity (E_0) and with impurity (E_I). Then, it is expressed as follows:

$$E_b = E_0 - E_I \tag{7}$$

The binding energy (BE) is obtained by solving numerically the Schrodinger equation taking into account a finite potential barrier height using finite element method. The boundary conditions are applied. They are satisfied by the following equations [30],

$$\left[\mathbf{n}\cdot\boldsymbol{\nabla}\left(\frac{\psi}{m^*_{e,b}}\right)\right]_{\mathrm{Barriers}} = \left[\mathbf{n}\cdot\boldsymbol{\nabla}\left(\frac{\psi}{m^*_{e,w}}\right)\right]_{\mathrm{QW}} \tag{8}$$

The mesh-grid of $3N+1$ points is considered for the investigated structure. Each layer discretized by different discretization step. For the barriers, the step is $h_b = L/N$ while for the well's regions it is given as $h_w = l/N$. Therefore, for $0 < k < N$, the mesh's nodes of single QW is given respectively as follows, left barrier is $z_k = k * h_b$, in the well region is $z_k = L + k * h_b$ and in the right barrier is given as $z_k = L + l + k * h_b$. The same algorithm has been used to create the mesh's nodes of double and triple coupled QWs. The discretization number used to perform this study is

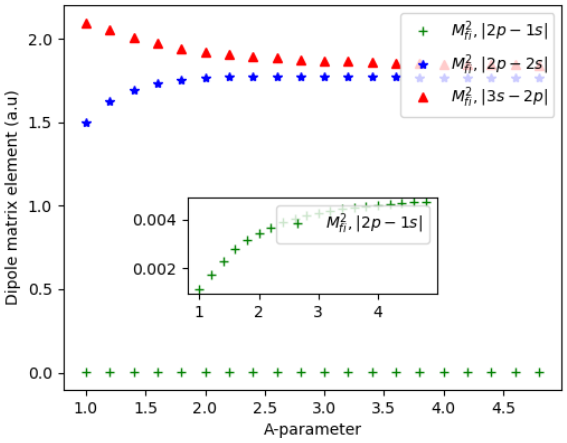

Figure 4. Square of the dipole matrix element of electron within the conduction band of InGaN/GaN QW as a function of the A-parameter. Without impurity and for l=L=1.5.

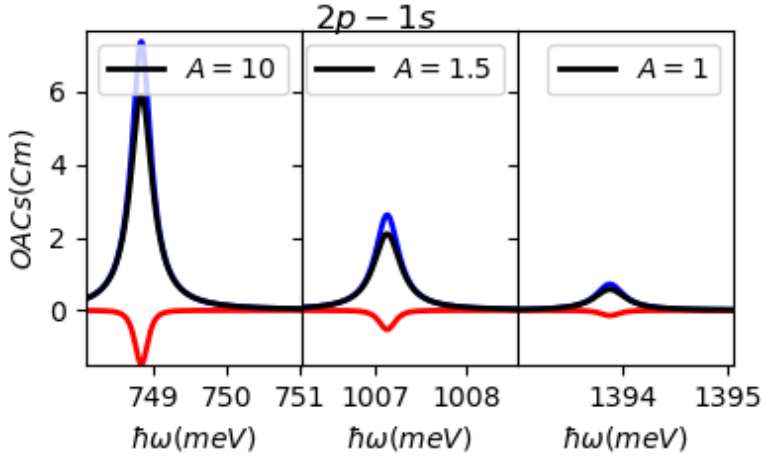

Figure 5. The linear (blue), third-order nonlinear (red) and total (black) optical absorption coefficients related to 2p→1s ISB transition versus the incident photon energy for three different values of the *A*-parameter with *l*=*L*=1.5.

N=50 points.

The first and the second derivatives wave functions are given respectively by:

$$\left.\frac{\partial^2\psi(z)}{\partial z^2}\right)_{zk} = \frac{\psi_{k+1}-2\psi_k+\psi_{k-1}}{(z_{k+1}-z_k)^2}$$

$$\left.\frac{\partial\psi(z)}{\partial z}\right)_{zk} = \frac{\psi_{k+1}-\psi_k}{z_{k+1}-z_k} \quad (9)$$

Although, after the electron's energy levels and their related wave functions have been calculated, the linear and third-order nonlinear optical absorption coefficients (OACs) for the ISB transitions between the ground state and excited states can be easily calculated within the compact density matric theory and it is given as follows [31, 32]:

$$\alpha^1(\omega) = \hbar\omega\sqrt{\frac{\mu}{\varepsilon_r^*\varepsilon_0}}\frac{\Gamma_{if}|M_{fi}|^2\rho}{(E_{fi}-\hbar\omega)^2+(\hbar\Gamma_{if})^2}, \quad (10)$$

$$\alpha(\omega,I) = -\sqrt{\frac{\mu}{\varepsilon_r^*}}\left(\frac{I}{2n_r^*\varepsilon_0 c}\right)\frac{4\Gamma_{if}|M_{fi}|^2\rho\hbar\omega}{[(E_{fi}-\hbar\omega)^2+(\hbar\Gamma_{if})^2]^2} \times\left[1-\frac{|M_{ff}-M_{ii}|^2}{4|M_{ff}|^2}\frac{3E_{fi}^2-4\hbar\omega E_{fi}+(\hbar\omega)^2-(\hbar\Gamma_{if})^2}{E_{fi}^2-(\hbar\Gamma_{if})^2}\right] \quad (11)$$

$$\alpha^T(\omega,I) = \alpha^1(\omega)+\alpha^3(\omega,I) \quad (12)$$

The transition energy between the allowed electronic states considered in this study (i.e., 1s, 2s, 2p and 3s) is given as $\Delta E_{fi} = E_f - E_i$, where f and i are consequently the final and initial states. The dipole matrix element between those is given as $|M_{fi}| = \langle\psi_i|ez|\psi_f\rangle$. It is important to mention that the optical transitions are possible between two deferent levels only if the selection rule ($\Delta l = \pm 1$) is satisfied. The different ingredients that we used to calculate our numerical results are given as follows: The electron density in the well region (InGaN) is $\rho(=2\times10^{26}\ \mathrm{m}^{-1})$. The incident electromagnetic intensity is $I(=1\times10^{10}\ \mathrm{W/m^2})$ and the relaxation time between implied electronic states, are given as $\Gamma_{fi} = 1/\tau_{fi}(=1\times10^{12}\ \mathrm{s}^{-1})$.

3. Results and discussion

In this paper, we aim to simplify our calculations by using the effective units. R_b^* and a_b^* used in this study are respectively the effective Rydberg and Bohr radius at the barrier region (GaN). The effective Rydberg $R_b^*(=m_b^*e^3/2(4\pi\varepsilon_b^*\hbar)^2)$ is used as unit energy while the effective Bohr radius $a_b^*(=4\pi\varepsilon_b^*\hbar^2/m_b^*e^2)$ is used as the unit of length. For

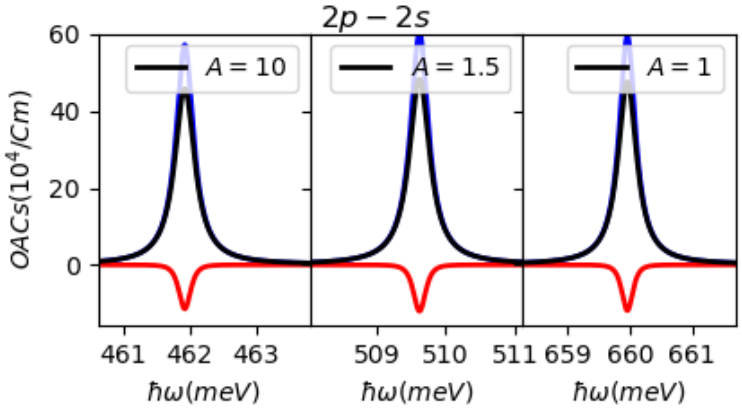

Figure 6. The linear (blue), third-order nonlinear (red) and total (black) optical absorption coefficients related to 2p→2s ISB transition versus the incident photon energy for three different values of the *A*-parameter with *l*=*L*=1.5.

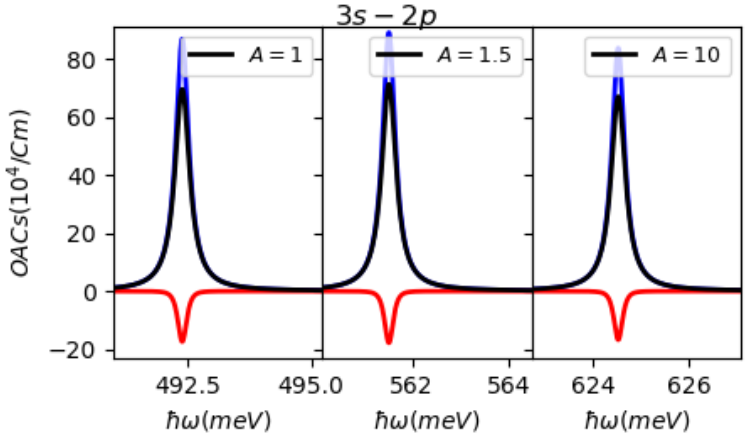

Figure 7. The linear (blue), third-order nonlinear (red) and total (black) optical absorption coefficients related to 3s-2p ISB transition versus the incident photon energy for three different values of the A-parameter with l=L=1.5.

L=l=1.5 and x=10%, R_b^*=29.13 meV and a_b^*=2.55 nm. It is important to notice that, all the numerical calculations were made for a fixed value of indium compositions equal to x=0.1 (10%) and an on-center impurity (fixed in the center of the well).

Before discussing the effect of A-parameter on the impurity binding energy the linear optical absorption coefficients, it would be important to evaluate the general behavior of potential profile of QW grown along the z-axis.

Figs. 1 (a-c) depicts the RHP confinement potentials associated with three different values of parameter A, the probability density distributions corresponding to energy levels of the lowest and three first excited states versus the z-coordinate. The A-parameter identifying conspicuously the shape of the potential is chosen as 1, 1.5 and 10. In case of A=1 a parabolic QW is formed whereas for $A \geq 1$ the potential begins to turn into a squared QW; it becomes perfectly squared for $A \geq 10$. Further increase in the A-parameter induces a deformation of the potential shape toward squared form and consequently the energies corresponding to 1s,2s,2p and 3s states are dropped. The important point that stands out is that the change in the shape of the potential is more evident for high values of the A-parameter where confinement is weaker, hence, the electron becomes more localized in the well region and then its energy decreases as a result.

Fig. 2 shows the variation of donor-impurity binding energies of 1s (red) and 2s (black) states as a function of the A-parameter. We see that the binding energy of both 1s and 2s states increases smoothly with respect to the A-parameter. As well known, the impurity binding energy increases or decreases because of the distance between the localization of the confined electron in the QWs and the impurity position. This behavior is a consequence of the enhancement in the overlap of the electron-impurity wave functions owing to the strengthening of the Coulombic interaction between the electron and the impurity located in the well center. Moreover, as expected, the ground state binding energy is always weaker than that of 2s-state for all values of the A-parameter and for both states, it becomes less sensitive to the variation of this A-parameter, especially for $A > 4$.

Fig. 3 (a,b) demonstrates the variation of the eletron energy levels and the its transition energy within the conduction band of a QW with respect to the A-parameter considering 2p→1s,2p→2s, and 3s→2p optical transitions. It is obvious that the increase in the A-parameter has considerably

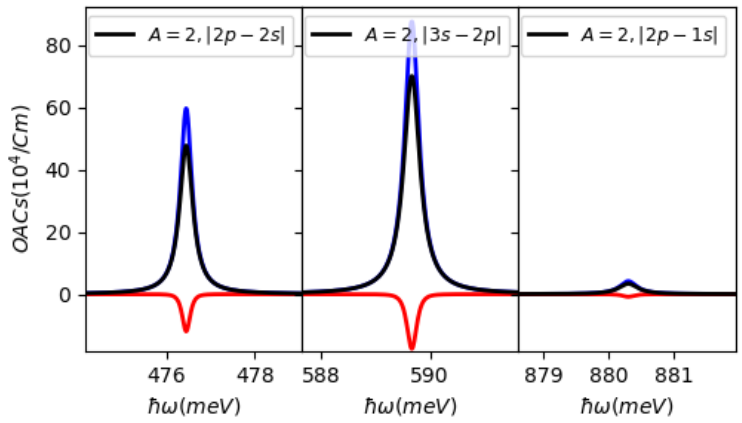

Figure 8. The linear (blue), third-order nonlinear (red) and total (black) optical absorption coefficients related to 2p→1s, 2p→2s, and 3s→2p ISB transitions versus the incident photon energy with l=L=1.5.

affected the energy levels as well as the electron transition energy. It is clearly that the energy levels of all the considered electron states decreases regarding the A-parameter and tends to a stable value for large values of A (>2). This is due to the fact that with increasing A the QW becomes wider and then the electron becomes less confined inside the well, therefore, its energy at all electronic states can only fall. A similar behavior have been noticed for the electron transition energy of the three considered optical transitions. According to the same figure (right panel), the transition energy decreases versus the A-parameter owing to the reduced confinement induced by the increase in the A-parameter. In addition, it appears that these energies of the transitions reach a stable value for value of A greater or equal to 2; also, it is noticed that energy transition associated with 3s-2p is the greatest compared to the others, except for small values of A-parameter A <1.5. This is due to the fact that the larger the parameter A is, the weaker the confinement becomes, which results in a lowering of the energy transition and vice-versa.

Figure 4 plots the variation of the square of the dipole matrix element resulting from the optical transitions 2p→1s, 2p→2s and 3s→2p as a function of the parameter A. It is observed that with the increase of the parameter A, the square of the dipole matrix bound to all the electronic states studied was affected. For the 2p→1s, 2p→2s transitions, it increases with respect to the parameter A while it decreases slightly for the 3s→2p transition. For all transitions, we obtained a stable dipole matrix element for large values of A (>2). This is explained by the fact that for small values of A, regardless the transition 2p→1s, the degree of quantum confinement decreases and then the overlap between the wave function of the electron being more important while it becomes much weaker and even constant for high values of A.

The results discussed above are essential for interpreting the behaviors of linear and nonlinear optical absorption coefficients (OACs) in the studied system. Due to the fact that these two concurrent parameters represent the two main parameters that control the behavior of OACs under external or internal forces. Because, the linear and nonlinear optical absorption coefficients are governed by the transition energy and the dipole matrix element. For instant, to discuss the optical properties related to different shapes investigated in this paper. It is crucial to mention that according to the Eqs.(11-13), the maximum value of the OACs occurs at energy $\hbar\omega = ((E_{21})^2 + (\hbar\Gamma_{21})^2)^{1/2}$ while their correspondent intensity is proportional to the quantity $((E_{21})^2 + (\hbar\Gamma_{21})^2)^{1/2}/\hbar\Gamma_{21}$. In the case that $E_{21} \gg \hbar\Gamma_{21}$, we get the simplified expression of the energy at which the maximum of the linear optical absorption coefficient occurs, i.e. $\hbar\omega \approx E_{21} + \hbar\Gamma_{21}$. Thus, the intensity at the maximum becomes proportional to $E_{21}/\hbar\Gamma_{21}$. Therefore, Figs. 5, 6 and 7 represent the effect of the parameter A on the behavior of the linear, nonlinear and total optical absorption coefficients versus the energy of the incident photons for three different ISB optical transitions (i.e., 2p→1s, 2p→2s and 3s→2p, respectively). According to these figures, the ISB optical absorption depends strongly on the A-parameter.

From Fig.5, it is noticed that the OACs have been remarkably improved while their resonance peaks positions have been shifted toward lower energy range (red-shifted) due to the significant enhancement of the dipole matrix element and the decrease in the transition energy associated 2p→1s ISB transition discussed in Figs. 3 and 4. Furthermore, it has been observed that the OACs associated with the other investigated ISB transitions (i.e., 2p→2s and 3s→2p) have been slightly dropped with increasing the parameter A, which is expected owing to the results discussed above in Figs. 3 and 4. However, the spectra position of OACs related to 2p→2s has been moved toward lower energies range (redshifted) while that of of OACs related to 3s→2p has been shifted toward higher energies range (blueshifted). The reason behind this behavior is for large values of A-parameter the confinement potential tends from a parabolic profile to a squared one, which reduces the quantum confinement and then leads to diminution of the electron transition energy related to 2p→2s ISB transition. Whereas, the transition energy corresponding to 3s→2p increases due to the fact that with increasing the A-parameter the energy 3s increases faster compared to that of 2p. This behavior in the ISB transition energies is associated with an augmentation of the dipole matrix element due to the improvement in the overlap between considered electronic states with increasing the A-parameter.

Similarly, In Fig.8, we depict the change of linear and nonlinear OACs related to 2p→1s, 2p→2s, and 3s→2p ISB transitions versus the incident photon energy. For a fixed confinement potential with A=2, we found that the absorption is highest by the 3s→2p ISB transition compared to the others. The reason for this is that with a fixed potential, the interaction strength and overlap between 3s and 2p is much larger than between the other states. Moreover, regardless of the 3s→2p ISB transition, it is observed that the 2p→1s ISB transition absorbs the highest energy around 880.5 meV, while the 2p→2s ISB transition absorbs the highest energy near 476.2 meV, which is in good agreement with the results reported in Fig.3.

4. Conclusion

To summarize, recall that we have theoretically studied the binding energy of the ground state and the first excited state of a donor impurity and the linear and nonlinear optical absorption coefficients related to 2p→1s, 2p→2s and 3s→2p ISB optical transitions in InGaN-based QW with a new finite modulated confinement potential called "RHP-potential". The Schrödinger equation has been solved numerically as part of the effective mass approximation using the finite element method. Our results reveal that varying the so-called A-parameter has a significant impact on both the binding energy of different states and the optical properties of QW. Furthermore, a redshift (blueshift) was obtained associated with a decrease (improve) in OACs related to the considered ISB optical transitions.

Data availability statement

All the files with tables, figures, and codes are available. The corresponding author will provide all the files in case they are requested.

Conflict of interest statement:
The authors declare that they have no conflict of interest.

References

[1] A. M. Ezpeleta. *Electronic Structure of Low-Dimentional System Analyzed by Angle-Resolved Photoemission Spectroscopy*. PhD Thesis, Aristotle University Of Thessaloniki (AUTH), Greece, 2002.

[2] N. Florini. *Study of the structure and mechanical behavior of low-dimentional III-V semiconductor heterostructures*. PhD Thesis, University of the Basque Country, 2021.

[3] S. Jagtap, P. Chopade, S. Tadepalli, A. Bhalerao, and S. Gosavi. "A review on the progress of ZnSe as inorganic scintillator". *Opto-Electron. Rev.*, **27**:90, 2019.

[4] I. R. Razali. *Development of a Continuous Microwave Reactor for the Production of Zinc Oxide*. PhD Thesis, Universiti Teknologi Malaysia, 2015.

[5] R. F. Farrow, S. S. P. Parkin, P. J. Dobson, J. H. Neave, and A. S. Arrott. *Thin Film Growth Techniques for Low-Dimensional Structures*. Springer Science and Business Media, 1th edition, 2013.

[6] B. Gil. *Low-dimensional nitride semiconductors*. Oxford University Press on Demand, 1th edition, 2002.

[7] R. Khordad, S. Goudarzi, and H. Bahramiyan. "Effect of temperature on lifetime and energy states of bound polaron in asymmetrical Gaussian quantum well". *Indian J. Phys.*, **90**:659, 2016.

[8] S. Mo, K. Guo, G. Liu, X. He, J. Lan, and Z. Zhou. "Exciton effect on the linear and nonlinear optical absorption coefficients and refractive index changes in Morse quantum wells with an external electric field". *Thin Solid Films*, **710**:138286, 2020.

[9] H. Sari, E. Kasapoglu, S. Sakiroglu, and I. Sökmen. "Position-dependent mass effects on the optical responses of the quantum well with Tietz–Hua potential". *Optik*, **178**:1280, 2019.

[10] E. Kasapoglu, H. Sari, I. Sökmen, J. A. Vinasco, D. Laroze, and C. A. Duque. "Effects of intense laser field and position dependent effective mass in Razavy quantum wells and quantum dots". *Phys. E Low-Dimens. Syst. Nanostructures*, **126**:114461, 2021.

[11] G.-H. Sun, C.-Y. Chen, H. Taud, C. Yá ñez Márquez, and S.-H. Dong. "Exact solutions of the 1D Schrödinger equation with the Mathieu potential". *Phys. Lett. A*, **384**:126480, 2020.

[12] S. Rajashabala and K. Navaneethakrishnan. "Effective masses for donor binding energies in quantum well systems". *Mod. Phys. Lett. B*, **20**:1529, 2006.

[13] E. Kasapoglu E. B. Al, S. Sakiroglu, C. A. Duque, and I. Sökmen. "Binding energy of donor impurity states and optical absorption in the Tietz-Hua quantum well under an applied electric field". *J. Mol. Struct.*, **1157**:288, 2018.

[14] M. Barati, G. Rezaei, and M. R. K. Vahdani. "Binding energy of a hydrogenic donor impurity in an ellipsoidal finite-potential quantum dot". *Phys. Status Solidi B*, **244**:2605, 2007.

[15] R. En-Nadir, H. El Ghazi, A. Jorio, and I. Zorkani. "Ground-state Shallow-donor Binding Energy in (In, Ga) N/GaN Double QWs Under Temperature, Size, and the Impurity Position Effects". *J. Model. Simul. Mater.*, **4**:1, 2021.

[16] R. Harris, J. Terblans, and H. Swart. "Exciton binding energy in an infinite potential semiconductor quantum well–wire heterostructure". *Superlattices Microstruct.*, **86**:456, 2015.

[17] H. El Ghazi, A. Jorio, and I. Zorkani. "Impurity binding energy of lowest-excited state in (In, Ga) N–GaN spherical QD under electric field effect". *Phys. B Condens. Matter*, **426**:155, 2013.

[18] M. Kirak, Y. Altinok, and S. Yilmaz. "The effects of the hydrostatic pressure and temperature on binding energy and optical properties of a donor impurity in a spherical quantum dot under external electric field". *J. Lumin.*, **136**:415, 2013.

[19] E. B. Al, E. Kasapoglu, S. Sakiroglu, H. Sari, and I. Sökmen. "Influence of position dependent effective mass on impurity binding energy and absorption in quantum wells with the Konwent potential". *Plasma Science and Technology*, **16**:552, 2014.

[20] F. Ungan, U. Yesilgul, S. Şakiroğlu, E. Kasapoglua, H. Sari, and I. Sökmen. "Effects of an intense, high-frequency laser field on the intersubband transitions and impurity binding energy in semiconductor quantum wells". *Phys. Lett. A*, **374**:2980, 2010.

[21] S. Ortakaya and M. Kirak. "Hydrostatic pressure and temperature effects on the binding energy and optical absorption of a multilayered quantum dot with a parabolic confinement". *Chin. Phys. B*, **25**:127302, 2016.

[22] B. Çakır, Y. Yakar, A. Özmen, M. Ö. Sezer, and M. Şahin. "Linear and nonlinear optical absorption coefficients and binding energy of a spherical quantum dot". *Superlattices Microstruct.*, **47**:556, 2010.

[23] M. Kırak, S. Yılmaz, M. Şahin, and M. Gençaslan. "The electric field effects on the binding energies and the nonlinear optical properties of a donor impurity in a spherical quantum dot". *J. Appl. Phys.*, **109**:094309, 2011.

[24] R. En-nadir, H. E. Ghazi, W. Belaid, A. Jorio, I. Zorkani, and H. Ş. Kiliç. "Ground and first five low-lying excited states related optical absorption in In.1Ga.9N/GaN double quantum wells: Temperature and coupling impacts". *Solid State Commun.*, **338**:114464, 2021.

[25] M. G. Burt. "The justification for applying the effective-mass approximation to microstructures". *J. Phys. Condens. Matter*, **4**:6651, 1992.

[26] M. H. Gazzah, B. Chouchen, A. Fargi, and H. Belmabrouk. "Electro-thermal modeling for InxGa1-xN/GaN based quantum well heterostructures". *Mater. Sci. Semicond. Process.*, **93**:231, 2019.

[27] R. En-nadir, H. El Ghazi, A. Jorio, and I. Zorkani. "Inter and intra band impurity-related absorption in (In, Ga) N/GaN QW under composition, size and impurity effects". *MATEC Web of Conferences*, **330**, 2020.

[28] H. El Ghazi, R. En-nadir, H. Abboudia, F. Jabouti, A. Jorio, and I. Zorkani. "Two-dimensional electron gas modeling in strained InN/GaN hetero-interface under pressure and impurity effects". *Phys. B Condens. Matter*, **582**:411951, 2020.

[29] R. En-nadir, H. El Ghazi, W. Belaid, A. Jorio, and I. Zorkani. "Intraconduction band-related optical absorption in coupled (In,Ga)N/GaN double parabolic quantum wells under temperature, coupling and composition effects". *Results Opt.*, **5**:100154, 2021.

[30] R. En-nadir, H. El Ghazi, A. Jorio, I. Zorkani, and H. Ş. Kiliç. "Intersubband optical absorption in (In,Ga)N/GaN double quantum wells considering applied electric field effects". *Journal of Computational Electronics*, **21**:111, 2022.

[31] H. El Ghazi, A. Jorio, and I. Zorkani. "Linear and nonlinear intra-conduction band optical absorption in (In, Ga) N/GaN spherical QD under hydrostatic pressure". *Opt. Commun.*, **331**:73, 2014.

[32] R. En-nadir, H. El Ghazi, A. Jorio, I. Zorkani, H. Abboudi, and F. A. Jabouti. "Numerical Study of Temperature and Electric Field Effects on the Total Optical Absorption Coefficient Related-Conduction-Subband Optical Transitions in InGaN/GaN Single Parabolic QW". *Fluid Dyn. Mater. Process.*, **18**:1253, 2022.